Journal of Alloys and Compounds 480 (2009) 510–515

Contents lists available at ScienceDirect

Journal of Alloys and Compounds

journal homepage: www.elsevier.com/locate/jallcom

A polyethylene glycol-assisted route to synthesize $Pb(Ni_{1/3}Nb_{2/3})O_3$-$PbTiO_3$ in pure perovskite phase

Yin Ye[a], Shuhui Yu[a], Haitao Huang[b,*], Limin Zhou[a,**]

[a] Department of Mechanical Engineering, The Hong Kong Polytechnic University, Hung Hom, Kowloon, Hong Kong
[b] Department of Applied Physics and Materials Research Center, The Hong Kong Polytechnic University, Hung Hom, Kowloon, Hong Kong

ARTICLE INFO

Article history:
Received 15 December 2008
Received in revised form 16 January 2009
Accepted 22 January 2009
Available online 6 February 2009

Keywords:
Ceramics
Ferroelectrics
Solid-state reactions
Thermal analysis

ABSTRACT

Ferroelectric relaxors $(1-x)Pb(Ni_{1/3}Nb_{2/3})O_{3-x}PbTiO_3$ (PNN-PT) with a composition ($x = 0.36$) near the morphotropic phase boundary (MPB) were prepared by a polyethylene glycol (PEG)-assisted solid-state reaction route. PEG with a molecular weight of 200 was introduced during the ball milling process of the raw oxide powders. XRD and TG/DSC results demonstrated that the interaction between PbO and PEG favors the transformation of lead-rich pyrochlore to lead-deficient pyrochlore, thus facilitating the formation of perovskite phase. Consequently, pure perovskite powders were synthesized at a relatively low temperature of 850 °C. Ceramics fabricated with the PEG-assisted route show a room temperature dielectric constant of 4987 and a maximum dielectric constant (at T_{max}) of 24,307 at a frequency of 1 kHz. The piezoelectric constant d_{33} measured was 460 pC/N.

1. Introduction

Ferroelectric relaxors of $Pb(B_{1/3}Nb_{2/3})O_3$ type, where B is either Mg, Ni, or Zn, and their solid solutions with $PbTiO_3$ (PT) have attracted much attention due to their excellent dielectric and piezoelectric properties [1–3]. Particularly, the solid solution of $Pb(B_{1/3}Nb_{2/3})O_3$ and PT, such as PNN-PT, shows outstanding dielectric and piezoelectric properties near the morphotropic phase boundary (MPB), where two or three phases coexist. Since the attractive dielectric and piezoelectric properties are only associated with pure perovskite phase, many efforts have been devoted to the synthesis of perovskite PNN-PT system. In the conventional solid-state reaction process, it is difficult to get a pure perovskite phase since undesired pyrochlore phases are easily formed at the initial stage of the solid-state reaction and are very difficult to remove [4,5]. Several attempts have been made to synthesize pyrochlore-free PNN-PT, such as the columbite method [6,7], acid-modified solid-state reaction [5], coating techniques [8] and spark plasma sintering [9].

Among various processing routes, the two-stage columbite method [10] is widely employed to stabilize lead-based relaxor perovskites. In the synthesis of PNN-PT via the columbite method, $NiNb_2O_6$ was first synthesized by sintering at 1000 °C for 6 h. It was then reacted with PbO and TiO_2 powders to form the perovskite phase by conventional solid-state reaction [6]. Although it is a reliable synthesis route for lead-based ferroelectric relaxors, the columbite method requires multiple steps of calcination and subsequent ball milling, thus increasing the complexity of the process. Actually, all of the methods mentioned above involve much more complicated processing procedures than the conventional solid-state reaction route.

In the present work, by simply introducing polyethylene glycol (PEG) into the ball milling process of the raw oxide powders of PbO, NiO, Nb_2O_5 and TiO_2, we have successfully synthesized 0.64PNN-0.36PT powders and ceramics with single perovskite phase at a relatively low temperature. The role of PEG played in the phase formation is discussed. The crystal structure and the dielectric properties of PNN-PT prepared by PEG-assisted route were characterized in comparison with those of PNN-PT prepared without the addition of PEG.

2. Experimental

2.1. Synthesis

PbO (99+%, International Laboratory, USA), NiO (Extra Pure Ni > 75%, International Laboratory, USA), Nb_2O_5 (99+%, International Laboratory, USA), and TiO_2 (99+%, International Laboratory, USA) were weighed according to the prescribed composition. Excess amount of PbO (5 at.%) was used in order to compensate the lead loss during calcination and sintering. The oxides were mixed with PEG (Extra Pure, International Laboratory, USA, molecular weight = 200) and followed by planetary ball milling in ethanol. The amount of PEG equals to that of PbO in molar ratio. After ball milling, the slurry was dried at 110 °C to evaporate ethanol and moisture, and burned at 300 °C for 4 h to decompose PEG. The burned powders were then

* Corresponding author. Tel.: +852 2766 5694; fax: +852 2333 7629.
** Corresponding author. Tel.: +852 2766 6663; fax: +852 2365 4703.
E-mail addresses: aphhuang@polyu.edu.hk (H. Huang), mmlmzhou@inet.polyu.edu.hk (L. Zhou).

0925-8388/$ – see front matter © 2009 Elsevier B.V. All rights reserved.
doi:10.1016/j.jallcom.2009.01.115

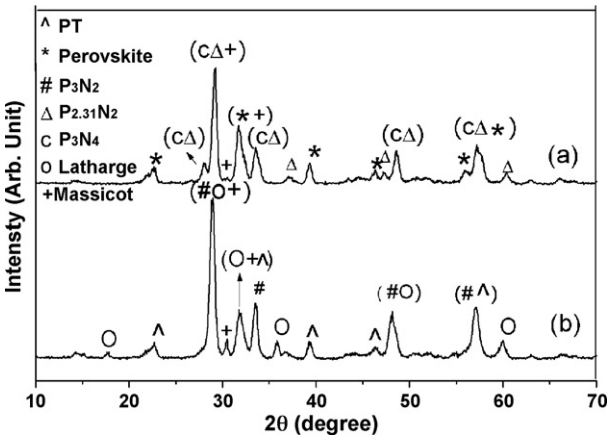

Fig. 1. XRD patterns of 0.64PNN-0.36PT powders derived from the oxides mixed (a) with and (b) without PEG200, both calcined at 600 °C for 4 h.

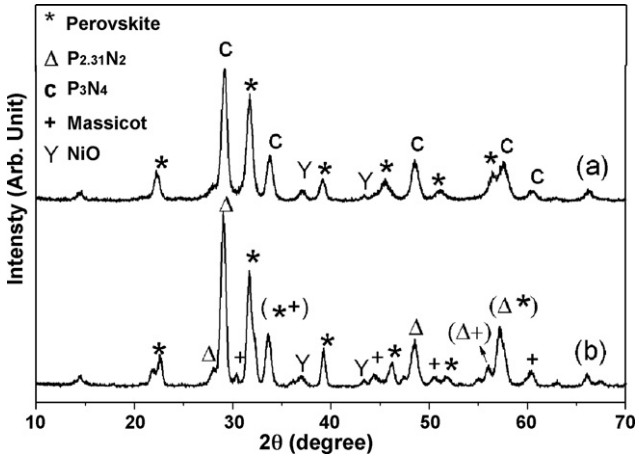

Fig. 2. XRD patterns of 0.64PNN-0.36PT powders derived from the oxides mixed (a) with and (b) without PEG200, both calcined at 750 °C for 4 h.

ground and calcined at 850 °C for 4 h. For comparison, another batch of samples were made by conventional solid-state reaction method where PEG was not used but similar ball milling, calcination and sintering procedures as those with PEG addition were adopted. The calcined powders were ground and pressed into pellets with polyvinyl alcohol (PVA) as the binder. The pellets were sintered at various temperatures ranging from 950 to 1150 °C for 2 h in a sealed alumina crucible under PbO atmosphere, which was provided by placing PbO powders inside the crucible.

2.2. Characterization

The crystal structures of the powders and ceramics were analyzed by using X-ray diffraction (XRD, X'pert System, Philips Electronic Instruments, Netherlands) with Cu Kα radiation. The data were collected within the 2θ range of 10–70° in steps of 0.04°, with an integration time of 1 s per step. The phases present here were identified using PDF-2 database [11]. The surface morphology of the PNN-PT ceramics was characterized by field emission scanning electron microscopy (FESEM, JEOL JSM-6335F). The thermal behaviors of the mixture of PEG and oxide powders after ball milling were examined by thermogravimetric and differential scanning calorimeter (TG/DSC, STA 409C, Netzsch, Germany) from room temperature up to 1100 °C with a heating rate of 10 °C/min. The thermal analyses of pure PEG and PbO were also conducted for comparison. Fourier transform infrared spectroscopy (FT-IR) of PEG samples was conducted on a PerkinElmer (Massachusetts, USA) 2000 system. A thin layer of PEG samples was painted on the KBr pellet (FTIR grade, Alfa Aesar Company) for FT-IR measurement in the range of 400–4000 cm^{-1}.

2.3. Dielectric measurements

For dielectric measurements, silver paste was painted onto both sides of the sample pellets as electrodes and baked at 650 °C for 15 min. The dielectric constant and loss tangent of the ceramics were measured as a function of temperature using an impedance analyzer (HP 4192A, USA), with a heating rate of 2 °C/min. Before the piezoelectric measurement, the electroded pellets were poled in silicone oil at 80 °C with an applied electric field of 3 kV/mm for 15 min. The piezoelectric constants d_{33} were measured using a piezo d_{33} meter (ZJ-38, Institute of Acoustics, Academia Sinica, China). The *P–E* hysteresis loops were measured with a Sawyer-Tower circuit.

3. Results and discussions

3.1. Crystal structure development

The XRD patterns of calcined powders derived from oxide precursors mixed with (or without) PEG and calcined at 600 °C are shown in Fig. 1. $Pb_3Nb_2O_8$ (denoted as P_3N_2, PDF 30-0712 [11]), tetragonal PbO (litharge, PDF 05-0561 [11]), and orthorhombic PbO (massicot, PDF 38-1477 [11]) are detected in calcined powders derived without the addition of PEG. In contrast, various pyrochlore phases such as $Pb_3Nb_4O_{13}$ (denoted as P_3N_4, PDF 25-0443 [11]) and $Pb_{2.31}Nb_2O_{7.31}$ (denoted as $P_{2.31}N_2$, PDF 72-1494 [11]), and orthorhombic PbO exist in calcined powders derived with the addition of PEG. The relative intensities of the diffraction peaks of PbO are lower in powders derived with PEG modification, which implies a larger amount of PbO is consumed in the formation of the perovskite and pyrochlore phases. Apart from pyrochlore phases and PbO, perovskite $PbTiO_3$ (denoted as PT, PDF 70-0747 [11]), which is generally formed at 500–550 °C [12], is also detected in both types of powders. However, perovskite $Pb(Ni_{1/3}Nb_{2/3}O_3)$ (denoted as PNN, PDF 34-0103 [11]) only presents in powders derived with PEG addition. The diffraction peak around 55.9°, which is characteristic for PNN, can only be observed in Fig. 1(a). The solid solution $Pb(Ni_{1/3}Nb_{2/3}O_3)$-$PbTiO_3$ (denoted as PNN-PT) may form as a result of the mutual solubility between PNN and PT. Since the majority of diffraction peaks of PNN, PT and PNN-PT are very close and overlap to each other, we do not differentiate them and mark them as perovskite phases in Fig. 1. Additionally, some diffraction peaks of different phases, especially for P_3N_4 and $P_{2.31}N_2$, are also close and overlap to each other (see Fig. 1). The overlapped diffraction peaks can be resolved by X-ray diffraction under slow scanning conditions utilizing PANalytical X'Pert HighScore software.

Fig. 2 reveals the XRD patterns of powders derived from oxide precursors mixed with (or without) PEG and heated at 750 °C for 2 h. In Fig. 2(a), P_3N_4 is the dominant phase without any detectable orthorhombic PbO, which suggests that with the assistance of PEG, all PbO reacts with other oxides to form pyrochlore or perovskite phases. In addition, similar to Fig. 1(a), the peak around 55.9° in Fig. 2(a) confirms the presence of PNN. In contrast, $P_{2.31}N_2$ and PT are the major phases in Fig. 2(b). A small amount of orthorhombic PbO can still be detected in powders derived without PEG addition.

Fig. 3 shows the XRD patterns of powders derived from oxide precursors mixed with (or without) PEG and calcined at 850 °C for

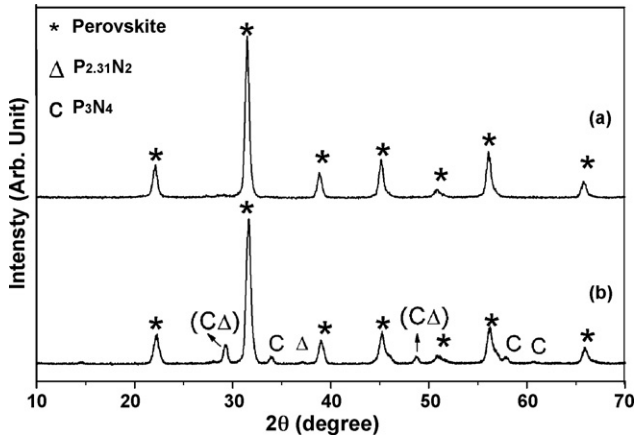

Fig. 3. XRD patterns of 0.64PNN-0.36PT powders derived from the oxides mixed (a) with and (b) without PEG200, both calcined at 850 °C for 4 h.

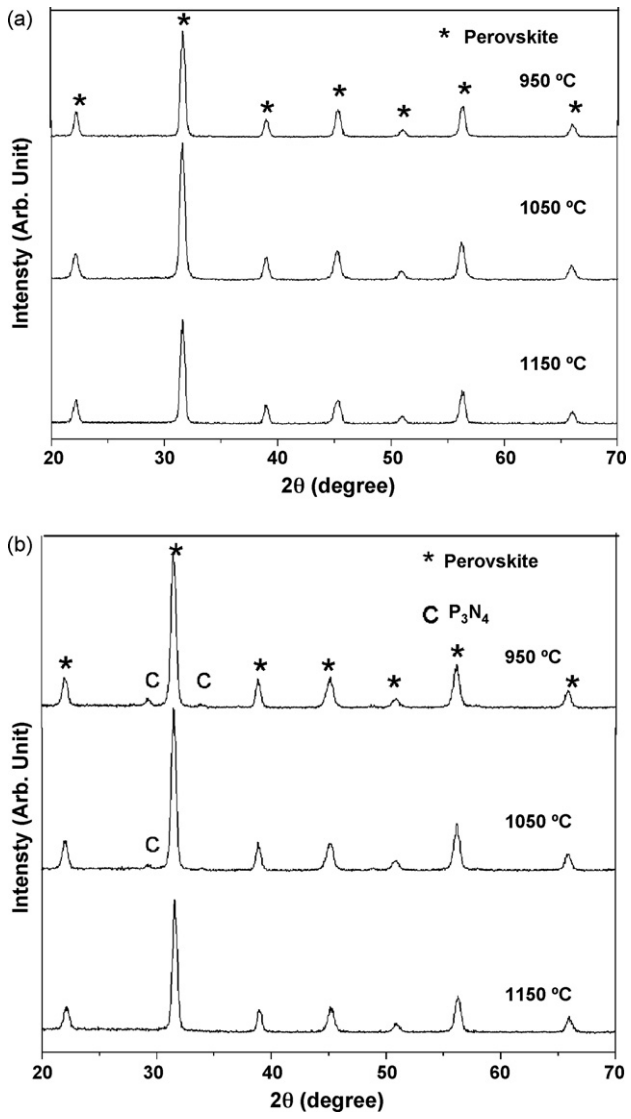

Fig. 4. XRD patterns of 0.64PNN-0.36PT ceramics derived from the oxides mixed (a) with and (b) without PEG200, which are sintered at 950, 1050 and 1150 °C for 2 h.

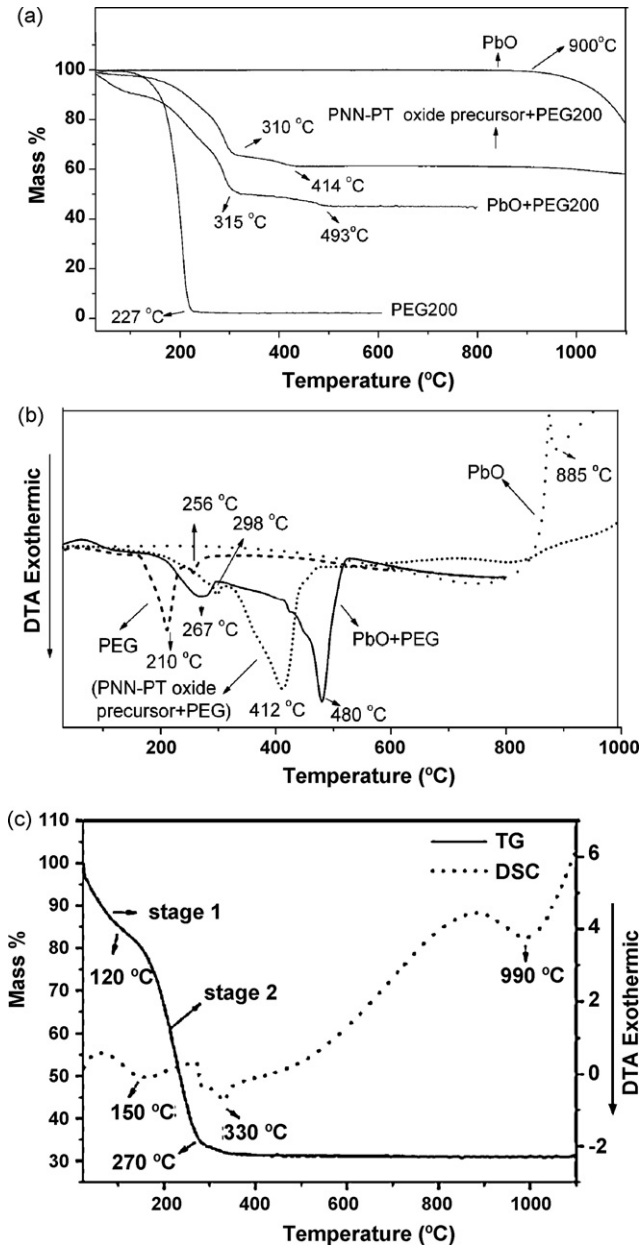

Fig. 5. (a) TG and (b) DSC curves for pure PEG200, PbO, the slurry of PbO with PEG200 and the mixture of PNN-PT oxide precursor and PEG200; (c) TG/DSC curves of the PEG mixed with NiO, Nb_2O_5 and TiO_2 oxide powders.

4 h. The perovskite phases dominate in both types of calcined powders. Pure perovskite phase is obtained in calcined powders derived with PEG. In contrast, $P_{2.31}N_2$ and P_3N_4 pyrochlores still exist in calcined powders derived without PEG. The above XRD results indicate that PEG promotes the formation of the perovskite phase.

The amount of the pyrochlore phases in the calcined powders can be roughly estimated by $I_{\text{pyrochlore}}/(\Sigma I_{\text{pyrochlore}} + I_{\text{perovskite}})$, where $I_{\text{pyrochlore}}$ is the intensity of the strongest diffraction peak of the pyrochlore phases, i.e. (2 2 2) for P_3N_4 and (0 2 7) for $P_{2.31}N_2$. $I_{\text{perovskite}}$ is the intensity of the (1 1 0) peak of the perovskite phase. Pyrochlore phases are estimated to be about 21% in powders calcined at 850 °C which is obtained via the conventional solid-state reaction method.

Ceramics were obtained by sintering at 950, 1050, and 1150 °C for 2 h for powders derived with (or without) the addition of PEG. XRD patterns (Fig. 4) reveal that pure perovskite phase is obtained in ceramics processed with PEG addition. However, pyrochlore P_3N_4 is not completely removed in ceramics without PEG addition, even after sintering at 1050 °C. About 4 and 2% P_3N_4 remains in ceram-

Table 1
Phase compositions of samples derived from oxide precursors mixed with and without PEG200.

Sample name	Phase compositions of samples without PEG	Phase composition of samples with PEG
Powders calcined at 600 °C for 4 h	P_3N_2, PbO (tetragonal), PbO (orthorhombic), PT	P_3N_4, $P_{2.31}N_2$, PbO (orthorhombic), perovskite phases (including PNN)
Powders calcined at 750 °C for 4 h	$P_{2.31}N_2$, PT, PbO (orthorhombic), NiO	P_3N_4, perovskite phases (including PNN), NiO
Powders calcined at 850 °C for 4 h	PNN-PT, P_3N_4, $P_{2.31}N_2$	PNN-PT
Ceramics sintered at 950 °C for 2 h	PNN-PT, P_3N_4 (4.4%)	PNN-PT
Ceramics sintered at 1050 °C for 2 h	PNN-PT, P_3N_4 (2.2%)	PNN-PT
Ceramics sintered at 1150 °C for 2 h	PNN-PT	PNN-PT

ics derived without PEG which are sintered at 950 and 1050 °C, respectively.

The detectable phases from the XRD patterns of powders and ceramics prepared with and without PEG are summarized in Table 1. According to previous studies [8,12], pyrochlore exists in many forms, including lead-rich tetragonal $Pb_3Nb_2O_8$ (P_3N_2), tetragonal $Pb_{2.31}Nb_2O_{7.31}$ ($P_{2.31}N_2$), and lead-deficient cubic $Pb_3Nb_4O_{13}$ (P_3N_4). It has been reported that in PNN-based system, tetragonal P_3N_2 and $P_{2.31}N_2$ tend to transform into cubic P_3N_4, which can further react with NiO and PbO to form the perovskite PNN at elevated temperatures [8,12]. Wakiya et al. [13] put forward that the full occupancy of A-sites of the pyrochlore structure by Pb(II) ions would be unstable due to the existence of $6s^2$ lone pair of Pb. Thus, lead-rich pyrochlore tends to convert to lead-deficient pyrochlore in PNN-PT system. Based on the XRD results and information from the previous studies, the sequence of reactions for the formation of the perovskite PNN-PT with (or without) PEG is proposed as follows:

$$Pb_3Nb_2O_8 \rightarrow Pb_{2.31}Nb_2O_{7.31} + 0.69PbO \quad (1)$$

$$2Pb_{2.31}Nb_2O_{7.31} \rightarrow 1.62PbO + Pb_3Nb_4O_{13} \quad (2)$$

$$PbO + TiO_2 \rightarrow PbTiO_3 \quad (3)$$

$$0.32PbO + \frac{0.32}{3}Pb_3Nb_4O_{13} + \frac{0.64}{3}NiO + 0.36PbTiO_3 \rightarrow 0.64PNN - 0.36PT \quad (4)$$

As illustrated in Table 1, in powders derived with PEG modification, $P_{2.31}N_2$ have been completely transformed into P_3N_4 after calcination at 850 °C. In contrast, for powders without PEG addition, $P_{2.31}N_2$ still exists after calcination owing to the incomplete transformation from P_3N_2 to P_3N_4 as shown in the reaction Eqs. (1) and (2). In the final stage, perovskite PNN-PT solid solution is obtained by reaction among P_3N_4, NiO, PbO, and PT.

Previous investigations on PMN-based systems [10,14] have shown that it is difficult for Mg atoms to be incorporated into the B-site rich pyrochlore structure of P_3N_4 to form the perovskite phase. However, it is generally accepted that P_3N_4 is the high temperature

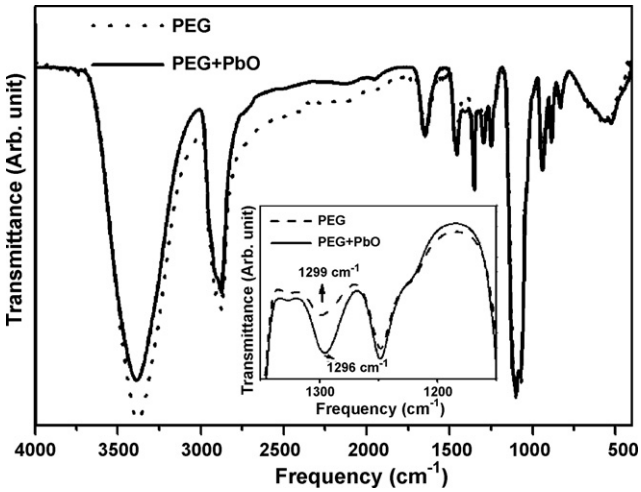

Fig. 6. FTIR spectra of pure PEG and PEG mixed with PbO. The inset shows an enlarged part of the spectra.

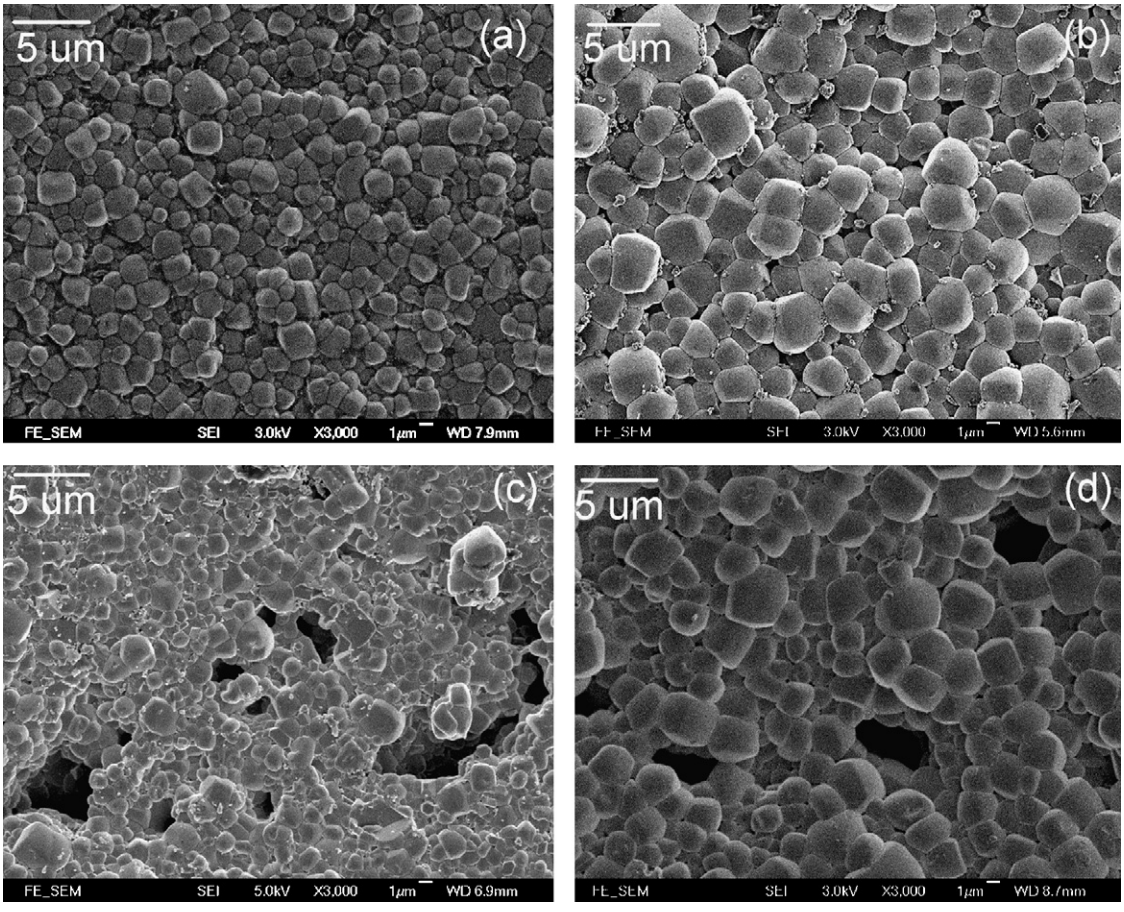

Fig. 7. Surface morphologies of PNN-PT ceramics sintered at 1050 °C [(a) with and (b) without PEG] and 1150 °C [(c) with and (d) without PEG], respectively.

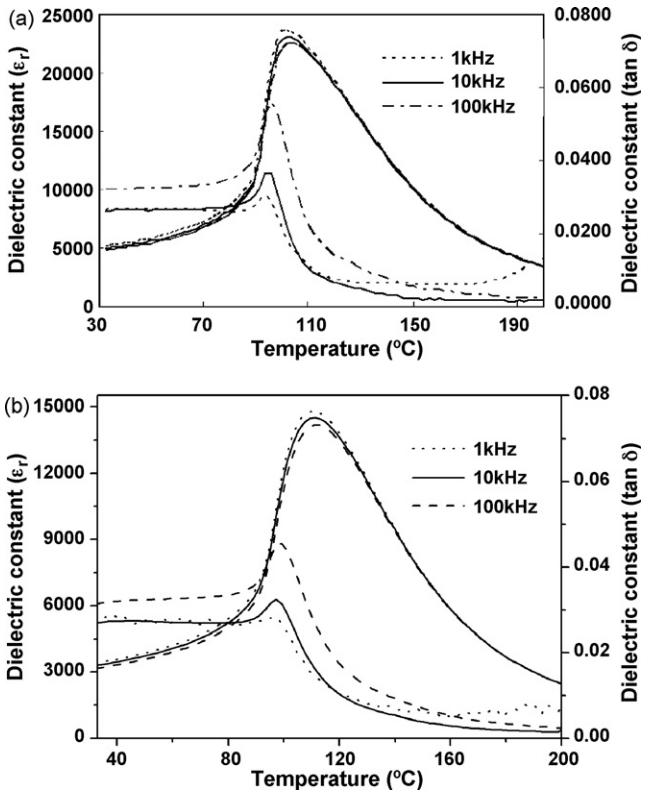

Fig. 8. Temperature dependence of dielectric constant (ε_r) and loss tangent ($\tan\delta$) at different frequencies for the ceramics derived from (a) with and (b) without PEG200.

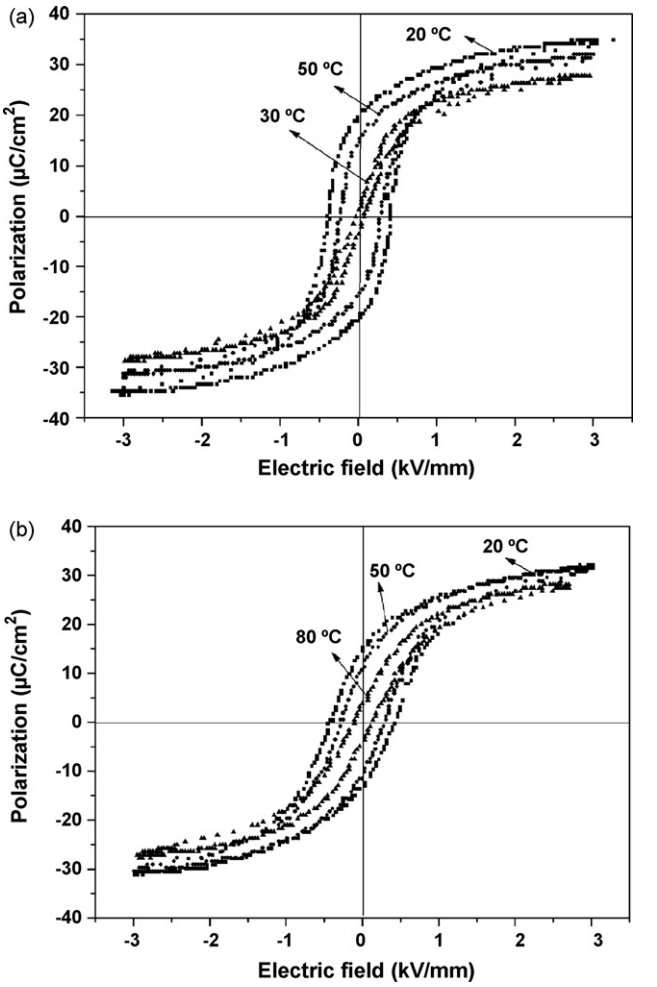

Fig. 9. Temperature dependence of the *P*–*E* hysteresis loop of ceramics derived (a) with and (b) without PEG200.

form of the pyrochlore phase in PNN-PT system, and it provides a basis for the formation of the perovskite phase. The difference between PMN-based system and PNN-based one lies in the reaction kinetics which depends on a number of factors, such as the reaction systems, surface states of raw materials, particle size, and processing method, etc.

The above discussion implies that the addition of PEG improves the reactivity of the system, thus lowering the formation temperature of P_3N_4 and facilitating the conversion from lead-rich pyrochlore to lead-deficient one. As a result, high temperature pyrochlore P_3N_4 forms in powders prepared with PEG after heat treatment at 600 °C and pure perovskite phase can be obtained in a subsequent calcination (Eq. (4)) at 850 °C.

According to previous studies [13,15,16], both the directional effect of $6s^2$ lone pair in Pb^{2+} and the oxygen deficiency lead to the formation of the pyrochlore phase. In PEG-modified PNN-PT system, we propose that the $6s^2$ lone pair electrons of Pb^{2+} in PbO tend to interact with the oxygen atoms from both the ether oxygen and hydroxyl in PEG structure, $OH–(CH_2CH_2O)_n–H$. Consequently, the directional effect of Pb^{2+} is weakened by the interaction between Pb^{2+} and PEG. Additionally, it is possible that some oxygen atoms from PEG still bond to Pb^{2+} even after the heat treatment at 600 °C and this provides an oxygen-rich environment, thus favoring the formation of the perovskite phase.

3.2. Thermal analysis

Fig. 5 exhibits the thermogravimetry (TG) and differential scanning calorimetry (DSC) curves of pure PEG200, PbO powder, PbO slurry with PEG200, and the mixture of oxides and PEG200. It is observed that PbO starts to lose its weight significantly at around 900 °C, a temperature slightly above its melting point. As shown in Fig. 5(a), almost all of the pure PEG200 has completely combusted at 227 °C. However, when PEG is mixed with the oxide precursor for PNN-PT, its decomposition is retarded and an additional small weight loss occurs in the temperature range of 310–414 °C. The whole weight loss from room temperature to 414 °C is about 38%, which approximately equals the weight percentage of PEG in the mixture of oxide precursor and PEG. This indicates that complete decomposition of PEG is retarded from 227 to 414 °C, when PEG and the oxide precursors are mixed. Similar phenomena are also observed for PbO slurry mixed with PEG. The retardation of the combustion of PEG suggests that there is interaction between PEG and oxides and the interaction is particularly strong between PEG and PbO. As a proof of concept, thermal analysis was conducted on mixture of PEG200 and oxides other than PbO. As shown in Fig. 5(c), the combustion of PEG is almost completed at 270 °C, well before the temperature for PEG mixed with PbO. This means that the interaction between PEG and PbO is the strongest, while the interaction between PEG and other oxides is weak.

As shown in Fig. 5(b), there are two exothermic valleys for pure PEG200 at 210 and 256 °C, respectively. They shift to higher temperatures, i.e., 298 and 412 °C, respectively, when PEG are mixed with PNN-PT oxide precursors. Similar shifts of exothermic valleys are also observed for PbO slurry mixed with PEG. The DSC curve of PbO is rather smooth within the temperature range of 200–500 °C, indicating no phase transformation or oxidization of lead (II) oxide within this temperature range. In the DSC curve of the mixture of oxide precursors and PEG, the relatively small valley at 298 °C corresponds to the initial stage of weight loss due to the partial decomposition of PEG chains below 310 °C. The deep valley at

412 °C is related to the second weight loss stage in the temperature range of 310–414 °C and can be ascribed to further decomposition of the residual broken chains of PEG connected to the surface of PbO particles.

3.3. FT-IR

Fig. 6 illustrates the FTIR spectra of pure PEG and the transparent suspension of the mixture of PEG and PbO after ball milling. These two spectra exhibit very similar patterns, but one difference should be noticed. The C–O–C asymmetric stretching vibration [$\nu_{COC(asym)}$] in pure PEG chains appears at 1299 cm^{-1}. It shifts to a lower wavenumber 1296 cm^{-1} when PEG is mixed with PbO. Since the frequency of $\nu_{COC(asym)}$ reflects the strength of the ether linkage [17], the frequency shift implies that the strength of the ether linkage is weakened by the interaction between PEG and PbO.

3.4. SEM

Fig. 7 illustrates the surface morphologies of PNN-PT ceramics processed with (or without) PEG and sintered at 1050 and 1150 °C, respectively. In Fig. 7(a) and (b), with PEG assistance, dense microstructure and uniform grains were observed in ceramics sintered either at 1050 or 1150 °C. The average grain size of the former ceramics is 1–2 μm, and it increased to 2–4 μm, when the ceramics were sintered at 1150 °C. In contrast, ceramics processed without PEG exhibit porous morphology and non-uniform grain size, ranging from 1 to 3 μm (Fig. 7(c)) for ceramics sintered at 1050 °C to 2–4 μm (Fig. 7(d)) for ceramics sintered at 1150 °C. It should be noted a small quantity of octahedral grains, which is cubic P_3N_4, can be observed in Fig. 7(c). The existence of octahedral P_3N_4 is also confirmed by the XRD results. Additionally, cubic crystals have a tendency to form octahedral morphology.

The above microstructure comparison leads to a conclusion that uniform and dense microstructure is easier to be obtained in ceramics derived from PEG-modified powders than in those derived without PEG. The improvement of the density and uniformity of PNN-PT ceramics significantly enhance their dielectric performance, which will be discussed below.

3.5. Dielectric properties

The temperature dependence of the relative dielectric constant (ε_r) and loss tangent ($\tan\delta$) of the PNN-PT ceramics processed with (or without) PEG and sintered at 1150 °C is illustrated in Fig. 8. For ceramics derived from PEG-modified powders, the relative dielectric constant and loss tangent at room temperature are 4987 and 0.022, respectively, at a measuring frequency of 1 kHz. The maximum dielectric constant (ε_{max}) is 24,307 at T_{max} (104 °C) when measured at 1 kHz. In contrast, for ceramics prepared without the addition of PEG, ε_r at room temperature is 3400 and ε_{max} is only 14,800, both of which are much lower than those of the PEG-modified ceramics. The decrease in dielectric constant in ceramics processed without PEG is partially due to the existence of a large number of porosities (see Fig. 7(d)), which also partially accounts for the increase of T_{max} to 111 °C [18]. Another reason for the decrease in dielectric constant and increase in T_{max} is the existence of P_3N_4 pyrochlore phase which is beyond the detection limit of XRD (see Fig. 4(b)). The pyrochlore phase results in a PNN/PT ratio lower than the nominal value of 64/36 and causes an increase in T_{max} [7]. For PEG-assisted PNN-PT ceramics, the piezoelectric constant d_{33} reaches 460 pC/N, which is also larger than that (280 pC/N) of ceramics without PEG modification in the present study.

The polarization versus electric field (P–E) hysteresis loops of PNN-PT ceramics sintered at 1150 °C and measured at different temperatures are shown in Fig. 9. The hysteresis loop of the ceramics processed with PEG shows better squareness than that of the ceramics processed without PEG. At room temperature, the remnant polarization (P_r) and the coercive field (E_c) reach 18.6 μC/cm^2 and 5.4 kV/cm, respectively. For ceramics prepared without PEG, P_r is lower but E_c is higher.

The above facts denote that the PEG-assisted route visibly improves the dielectric and piezoelectric properties of PNN-PT ceramics which is resulted from the enhanced density and pure perovskite phase of the ceramics.

4. Conclusions

By introducing PEG200 into the ball-milling process of the conventional solid-state reaction route, 0.64PNN-0.36PT powders and ceramics with a pure perovskite phase are successfully synthesized in this study. Compared to the columbite method, the current method can produce pure perovskite phase at a relatively low calcination temperature of 850 °C. The interaction between PEG and PbO is thought to favor the formation of the perovskite phase. With PEG modification, the dielectric and piezoelectric properties of sintered PNN-PT ceramics are greatly improved. Moreover, the density of sintered ceramics is also increased in samples with PEG modification and this in turn, contributes to the improvement of properties.

Acknowledgements

This work is supported by the Research Grants Council of the Hong Kong Special Administrative Region, China (Projects No: PolyU5279/04E and PolyU5171/07E) and the Hong Kong Polytechnic University (Grant No: RGNB and A-PB0L).

References

[1] J.C. Ho, K.S. Liu, I.N. Lin, J. Mater. Sci. 28 (1993) 4497–4502.
[2] L.B. Kong, J. Ma, H. Huang, R.F. Zhang, Mater. Res. Bull. 37 (2002) 2491–2498.
[3] L.B. Kong, J. Ma, H. Huang, R.F. Zhang, T.S. Zhang, J. Alloy Compd. 347 (2002) 308–311.
[4] N. Uekawa, T. Sukegawa, K. Kakegawa, Y. Sasaki, J. Am. Ceram. Soc. 85 (2002) 329–334.
[5] K. Kusumoto, T. Sekiya, Ferroelectrics 240 (2000) 327–334.
[6] Z.R. Li, X. Yao, Mater. Sci. Lett. 20 (2001) 273–275.
[7] Z.R. Li, L.Y. Zhang, X. Yao, J. Mater. Res. 16 (2001) 834–836.
[8] P.H. Xiang, N. Zhong, X.L. Dong, J. Am. Ceram. Soc. 88 (2005) 239–242.
[9] K.P. Chen, C.W. Li, C. Lei, X.W. Zhang, Y. Huang, J. Mater. Sci. Lett. 21 (2002) 1785–1787.
[10] S.L. Swartz, T.R. Shrout, Mater. Res. Bull. 17 (1982) 1245–1250.
[11] PDF-ICDD. PCPDFWIN Version 2.4, June 2003, International Centre for Diffraction Data, 2003.
[12] O. Babushkin, T. Lindbäck, J.C. Luc, J. Eur. Ceram. Soc. 18 (1998) 737–744.
[13] N. Wakiya, B.H. Kim, K. Shinozakik, J. Ceram. Soc. Jpn. 102 (1994) 612–615.
[14] O. Bouquin, M. Lejeune, J.P. Boilot, J. Am. Ceram. Soc. 74 (1991) 1152–1156.
[15] C. Cascales, I. Rasines, P.G. Casado, Mat. Res. Bull. 20 (1985) 1359–1365.
[16] S. Yu, H. Huang, L.M. Zhou, Chem. Mater. 19 (2007) 2718–2720.
[17] J. Grainger, W. Reddy, D.G. Patterson, Appl. Spectrosc. 42 (1988) 643–655.
[18] T. Hiroshima, K. Tanaka, T. Kimura, J. Am. Ceram. Soc. 79 (1996) 3235–3242.